






## RESEARCH ARTICLE

# Structure and durability of opal crystallized glass plates

Léa Brunswic<sup>1</sup>  | Frédéric Angeli<sup>1</sup>  | Laurent Gautron<sup>2</sup> |  
Thibault Charpentier<sup>3</sup>  | Stéphane Gin<sup>1</sup>  | Pierre Asplanato<sup>1</sup> | Huseyin Kaya<sup>4</sup> |  
Seong H. Kim<sup>4,5</sup> 

<sup>1</sup>CEA, DES, ISEC, DPME, Université de Montpellier, Bagnols-sur-Cèze Cedex, France

<sup>2</sup>Laboratoire Géomatériaux et Environnement (LGE, EA 4508), Université Gustave Eiffel, Marne la Vallée Cedex 2, France

<sup>3</sup>CEA, CNRS, NIMBE, Université Paris-Saclay, Gif-sur-Yvette cedex, France

<sup>4</sup>Department of Materials Science and Engineering, The Pennsylvania State University, University Park, Pennsylvania, USA

<sup>5</sup>Department of Chemical Engineering and Materials Research Institute, The Pennsylvania State University, University Park, Pennsylvania, USA

**Correspondence**

Frédéric Angeli, CEA, DES, ISEC, DPME, Université de Montpellier, Marcoule, 30207, Bagnols-sur-Cèze Cedex, France.  
Email: [frederic.angeli@cea.fr](mailto:frederic.angeli@cea.fr)

**Funding information**

French Agency for Research, Grant/Award Number: 18-CE08-0025

**Abstract**

An opal crystallized glass plate, obtained from the addition of fluorine to a soda-lime base, has been structurally characterized and altered in food contact like conditions. The investigations on the pristine glass evidenced the nature of CaF<sub>2</sub>, BaF<sub>2</sub>, and NaF crystalline phases. Overall a continuum of fully vitreous to glass-ceramic material was noticed with different morphology: the top surface that resembles a soda-lime glass which was prepared as a slab and the highly crystallized bulk using powder. Powder and slab were altered together at 70°C in acetic acid 4% (v/v) imposing a pH of 2.4 for 231 days to 3 years. The bulk powder alteration was characterized by a predominant hydrolysis mechanism impacting the crystals and the glassy matrix, leaving no remaining altered layer at the surface whereas a 1.25 μm thick alteration layer was observed on the top surface of the plate after 231 days of alteration. The mechanisms for the formation of this altered layer as well as the differences between the powder, representative of the bulk opal crystallized glass, and the slab that remains the actual surface in contact with edibles are discussed in the article.

**KEYWORDS**

alteration, glassware, kinetics, opal glass

## 1 | INTRODUCTION

Opal crystallized glass is a choc resistant, heat resistant, and endlessly tailored material widely used for tableware and cookware. This unique material brings together two opposite features of material sciences: an amorphous matrix, that can be qualified as glass, and well-ordered crystals embedded in the matrix, making it a glass-ceramic. Three different crystalline phases originating from the addition of fluorine to a soda-lime base composition are

bringing color and opaqueness to this material. Opal glass items are used repeatedly on a daily basis to hold in edible contents requiring sturdy and lasting durable properties, especially regarding food contact.

All opal plates start with a gob of fused glass dropped at the center of a steel mold and immediately centrifuged to reach the desired size and thickness of glass. From a macroscopic point of view, it forms a white plate, almost opaque, with two large and almost flat surfaces: the top and the bottom.

This is an open access article under the terms of the [Creative Commons Attribution-NonCommercial-NoDerivs](https://creativecommons.org/licenses/by-nc-nd/4.0/) License, which permits use and distribution in any medium, provided the original work is properly cited, the use is non-commercial and no modifications or adaptations are made.

© 2024 The Author(s). *International Journal of Applied Glass Science* published by American Ceramics Society and Wiley Periodicals LLC.

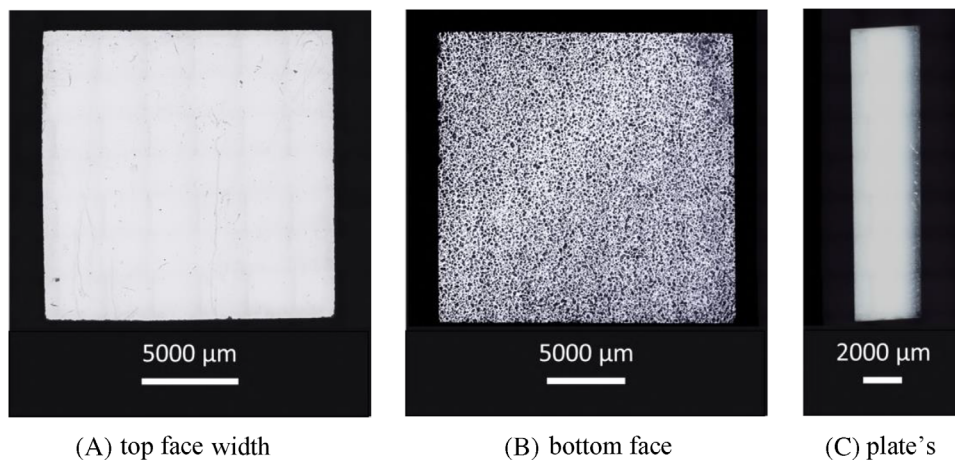


**FIGURE 1** Optical micrographs of an opal crystallized glass slab cut from the middle of a plate with (A) the top face of the plate with a smooth aspect, (B) the bottom face which exhibits important roughness, and (C) a view of the total width of the plate with the smooth top side along the left long side and the rough bottom side along the right long side.

The International Standards Organization has established acetic acid 4% (v/v) as food substitute for testing standards shedding the light on the lack of scientific knowledge on glassy matrices' chemical durability under acidic conditions and specifically glass-ceramics.<sup>1</sup> In order to better understand how opal glass alters, we studied both the microstructure and the chemical durability of samples of a commercial opal crystallized glass as above described. Results were interpreted relying on in-depth knowledge of the chemical durability of silicate glasses. Indeed, this topic is studied for numerous industrial applications or fundamental processes at play on earth: long-term nuclear waste disposal,<sup>2</sup> conservation of heritage materials,<sup>3</sup> wool glass for isolation,<sup>4</sup> biocompatibility for bone repair,<sup>5</sup> or even ocean geochemistry.<sup>6</sup>

In brief, silicate glass alters in contact with water following various mechanisms (ion-exchange, covalent bonds hydrolysis, condensation reactions leading to an amorphous, hydrated and porous layer, precipitation of secondary phases) leading to element release into the fluid and change of the glass surface composition and properties. The importance of the alteration mechanisms above listed on the whole alteration process depends on both intrinsic parameters (glass composition<sup>7</sup> and microstructure<sup>8</sup>) and environmental parameters (temperature, solution composition, pH, fluid renewal rate...). For details, one can refer on recent reviews on glass durability.<sup>9–12</sup>

Structural disorder related to the thermal history of glass can modify its leaching properties.<sup>13</sup> In partially crystallized glass, the effect of the cooling rate is even more significant as it directly influences the crystallization rate and is therefore likely to highly modify the release of elements from the glass.<sup>14,15</sup> The industrial process of manufacturing opal glass plates in a mold leads to different cooling between the surface in contact with the mold

and the surface in contact with the air. It is then interesting to better understand how each part of this glass behaves under acidic conditions (bulk and surfaces) and to relate them to the structural modifications induced by the cooling of the glass.

In this study, a plate made of opal glass has been fully characterized and its durability has been studied. Based on standardized test ISO 7086 the alteration of bulk powder and a slab representative of the actual surface of the plate were altered together at 70°C in acetic acid 4% (v/v) for 3 years and monitored through characterizations of the surface and the alteration solution. Comparison between the behavior of the powder and slab highlights the rate-limiting mechanisms and alteration kinetics that depend on the material's microstructure.

## 2 | RESULTS AND DISCUSSION

### 2.1 | Pristine glass features

#### 2.1.1 | Composition and morphology

Optical microscope images of both sides and the width of the plate are presented in Figure 1. The bottom side of the plate lies in contact with the steel mold during the shaping process, resulting in two major differences between the top and the bottom sides: (i) the bottom side exhibits a microscopic roughness visible in Figure 1B, which is not the case of the top face that remains smooth (Figure 1A) and (ii) the cooling rates of the two sides are different as the top side is only in contact with the atmosphere which has a poor calorific capacity, especially compared to the steel mold, strongly impacting the crystallization process in the glass. This process results in plates with two nonequivalent faces and macroscopic heterogeneous distribution of the

**TABLE 1** Bulk glass composition in molar percent of oxide analyzed by inductively coupled plasma atomic emission spectroscopy (ICP-AES) after complete acidic dissolution.

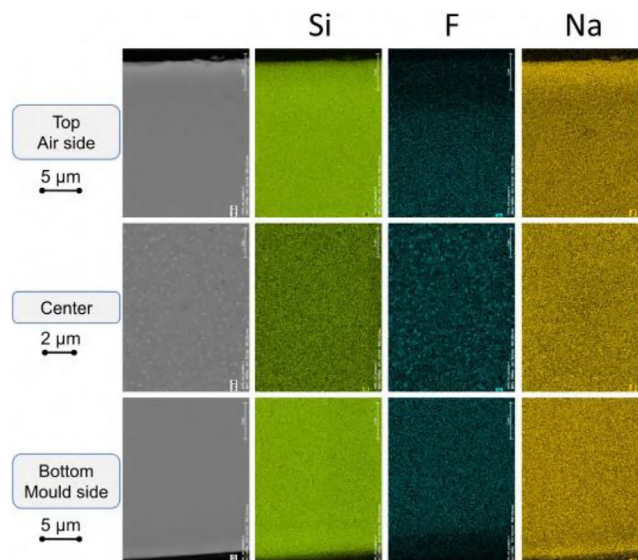
Oxide	SiO <sub>2</sub>	Na <sub>2</sub> O	Al <sub>2</sub> O <sub>3</sub>	CaO	BaO	K <sub>2</sub> O	F <sub>2</sub>
Mol%	73.6	11.9	4.8	2.2	0.8	1.0	5.7

The relative uncertainty on these measurements is considered to be 20%.

crystalline phases widthwise. The glass structure before alteration is briefly described for purposes of comparison with the after alteration case. To embrace the diversity found in a sample plate this material was studied under two different forms: powder, corresponding to the average bulk, dominated by a glass-ceramic structure, and a slab cut from a plate and representative of the real case surface in contact with edibles. The composition of the bulk powder was determined by complete acidic dissolution and is given in Table 1.

### 2.1.2 | Scanning electron microscopy

The observation of a cross-section of a plate including the top and bottom faces shows different degrees of heterogeneity in terms of phases and distribution of these phases although the distribution of silicon, the main glass constituent, seems homogeneous throughout the sample. Crystals are embedded in a glassy matrix with different glass/crystals ratios depending on the distance to the top. The first observable crystals under these conditions are located 9 μm below the top surface, and their measured diameter is about 60 nm. Twenty micrometer below the surface, the average diameter of the crystals measured is increasing to 90 nm, in correlation with the mapping of fluorine, given in Figure 2, which appears completely depleted from the first 7 μm area and then gradually increasing as the crystal's diameter grows. The larger crystals are found in the center region spreading across the majority of the sample's breadth and measured up to 200 nm with a homogeneous distribution within the glassy matrix. No crystals are observed in the 100 μm closest to the bottom surface although the chemical mapping clearly shows the presence of F except for the last 3 μm. As a matter of fact, crystals with a diameter inferior to 50 nm can not be detected through this technique but the presence of these nanocrystals is answered later on thanks to solid state nuclear magnetic resonance (NMR) spectroscopy data. Sodium also shows a very peculiar gradient of distribution near the top surface with the outermost 4 μm exhibiting a strong presence of Na followed by a depleted region shifting through a smooth gradient to the base level of sodium found throughout the majority of the sample. The same pattern is observed from the bottom face spreading on a twice smaller area.

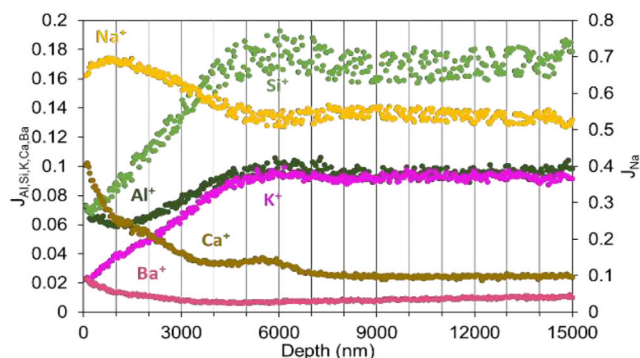
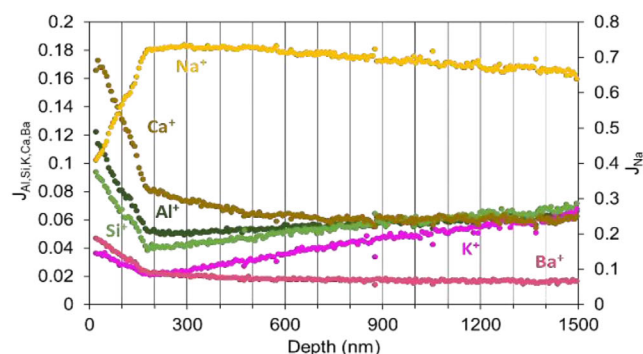


**FIGURE 2** Scanning electron microscopy (SEM) micrographs (backscattered electrons) of the top, middle, and bottom regions of a cross-section from an opal crystallized glass plate and energy-dispersive X-ray spectroscopy (EDS) mapping of Si, F, and Na from the same regions.

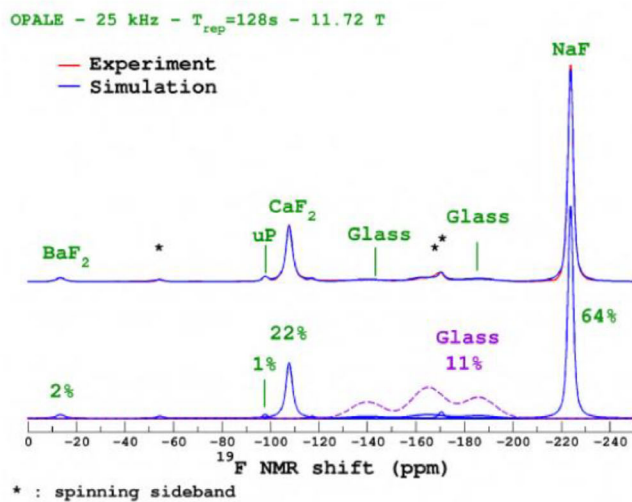
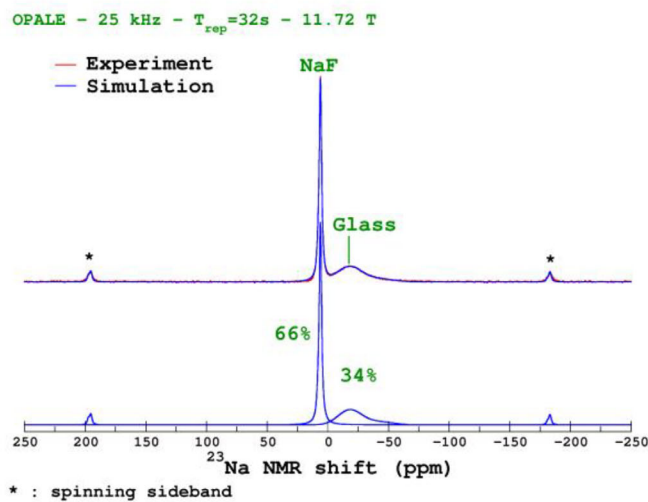
### 2.1.3 | ToF-SIMS

In accordance with scanning electron microscopy (SEM), time of flight secondary ion mass spectroscopy (ToF-SIMS) shows for the smooth face analysis, a top 4 μm thick layer enriched in Na, Ba, and Ca as observed in Figure 3A. Moreover Si, Al, and K are depleted from the top 6 μm of the sample. At least for Si, this result is in agreement with the SEM chemical mapping of the top air side of the material (Figure 2). However it must be kept in mind that ToF-SIMS profiles are not quantitative as the ionization yields depend both on the element and the local matrix, and no internal standard element could be used, great variations of intensity do not necessarily account for great concentration changes in the glass.

ToF-SIMS analyses sheds light more precisely on the first hundreds of nanometers that could not be observed via SEM microscopy. Results show a very peculiar distribution of elements among the first 200 nm. Figure 3B presents a similar trend for all elements analyzed except Na: steeply decreasing gradients until 180 nm depth followed by a stabilization of the signals slowly starting to show the trends confirmed by the deeper analysis on Figure 3A. On the opposite, Na is quite depleted from the top 180 nm before entering the enriched area observed between 0 and 4 μm in Figure 3A. Interestingly, it can be seen that the first 180 nm layer is hydrated as seen on H, SiOH, and Na profiles (available in Figure S13). The depletion of Na could be seen as the result of first stage atmospheric alteration due to the

(A) ToF-SIMS profiles until 15  $\mu\text{m}$ (B) ToF-SIMS profiles until 1.5  $\mu\text{m}$ 

**FIGURE 3** Time of flight secondary ion mass spectroscopy (ToF-SIMS) profiles obtained from the analysis of the smooth face of a pristine opal crystallized glass plate. The ions displayed represent the species detected by the mass spectrometer after sputtering. The signals are normalized to the total intensity. Signals from Al, Si, Ca, Ba, and K are read on the left hand Y-axis and signal from Na is read on the right hand Y-axis.

(A)  $^{19}\text{F}$  MAS NMR(B)  $^{23}\text{Na}$  MAS NMR

**FIGURE 4** Experimental and simulated magic-angle spinning nuclear magnetic resonance (MAS NMR)  $^{19}\text{F}$  (A) and  $^{23}\text{Na}$  (B) obtained from pristine opal glass powder at 25 kHz and 11.72 T. The glass contribution in figure A (purple dashes) is zoomed. The fitting procedure (simulation) is detailed in Section 4.2.

storage of the glass<sup>3,16</sup> between its production and the start of the experiment.

### 2.1.4 | NMR spectroscopy

The powder obtained from the crushing, grinding, and sieving of a commercial plate was analyzed by magic-angle spinning (MAS) NMR spectroscopy giving an overview of the average predominating structure of opal crystallized glass plates. The optical properties of the same opal crystallized glass were studied by Rio et al.<sup>17</sup> and it was

determined that crystals represented 8 wt% of the material, otherwise constituted of 92 wt% of glassy matrix. The  $^{19}\text{F}$  MAS NMR spectra collected from pristine opal crystallized glass powder, represented in Figure 4A, show the presence of three crystallized compounds: NaF,  $\text{CaF}_2$ , and  $\text{BaF}_2$ , and a glassy amorphous matrix. This technique allows the quantification of these phases by fitting the peaks yielding a distribution of F and Na among the different phases that is reported in Figure 4A,B, respectively. Eleven percent of the total fluorine molar content is found in the glassy matrix, as shown in the zoomed spectra with purple dashes, explaining the bottom region with chemical



**TABLE 2** Proportions of crystallized phases (% crystal) and of cations present in a crystallized phases (% of cations).

	NaF	CaF <sub>2</sub>	BaF <sub>2</sub>	
% Crystal	64	22	2	
	Ca	Ba	F	Na
% Cations in crystals	81	20	89	43

mapping of F but no crystals in Figure 2 as part of fluorine is dissolved in the glassy matrix. The highest contribution of F goes for the NaF crystals with 64% of F consumed far from the 22% for CaF<sub>2</sub> and 2% for BaF<sub>2</sub> crystals. One percent of the total area of the spectra occurred as a line at -98 ppm and was assigned as an unknown phase (uP). It is most probably a very little fraction of CaF<sub>2</sub> forming a solid solution with another cation or a lone phase arising from the presence of very small amounts of impurities in the glass forming its own phase.

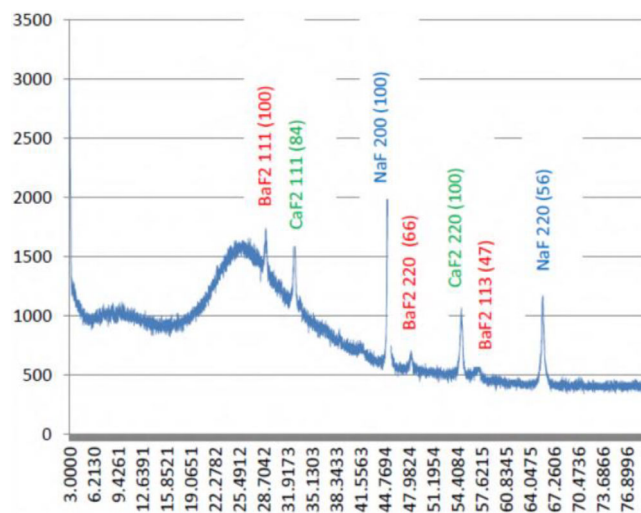
Considering the <sup>23</sup>Na spectrum (Figure 4B), the fitting yields 34% for the glassy matrix and 66% for NaF contribution, accounting for all the transitions detected, namely, central and satellite, of the Na sites from NaF and only the central transitions from the Na sites in the glassy matrix. The normalization of the contribution from the NaF crystals to the intensity of the central transition only for the appropriate  $\ell$  and  $m$  value<sup>18</sup> gives a final output of 44% for the NaF crystallized phase and 56% of Na located in the glassy matrix.

The high sensibility of <sup>19</sup>F nucleus provides fine information on fluorine and earth-alkali elements distribution: most of the Ca content belongs to crystals, 81% of Ca is incorporated in CaF<sub>2</sub>, as opposed to barium with only 20% found in BaF<sub>2</sub>. Although F remained the main constituent of the crystallized phase, part of F is incorporated in the glassy matrix. Data regarding sodium emerged from the cross-checking of <sup>19</sup>F and <sup>23</sup>Na MAS NMR fits, both data sets agreeing on 43% of the total sodium found in the NaF crystals and 57% Na in the matrix lowering the Na<sub>2</sub>O content of the glassy matrix to 6.7 mol%. The main results are summarized in Table 2.

Aluminum has also been investigated with <sup>27</sup>Al MAS NMR demonstrating the presence of Al in the glassy matrix only and almost exclusively under tetrahedral configuration (Figure S14). A very small contribution of sixfold coordinated Al atoms was noticed and estimated to be inferior to 1% with no impact on the global structure.

### 2.1.5 | X-ray diffraction

The pristine opal glass was also characterized by X-ray diffraction (XRD): the XRD pattern is presented in Figure 5. It is typical of glass embedding crystals, with

**FIGURE 5** X-ray diffraction pattern obtained from the pristine opal glass powder. The phases BaF<sub>2</sub> (JCPDS 04-0452), CaF<sub>2</sub> (JCPDS 87-0971), and NaF (JCPDS 36-1455) are identified along with a glassy phase.

a broad bump characteristic of the vitreous matrix and narrow peaks arising from crystal phases. The three expected crystals were identified: NaF, CaF<sub>2</sub>, and BaF<sub>2</sub>, from the crystal structures of villiaumite (halite-type), fluorite and frankdicksonite (fluorite-type), respectively, as referenced on the website MinCryst (<http://database.iem.ac.ru/mincryst/>).

### 2.1.6 | Transmission electron microscopy

Transmission electron microscopy (TEM) was used to answer some questions as asked above, in particular on the presence of crystals on a nanometric scale and on the variations in composition over distances of the order of a few hundred nanometers. First, we can observe and identify the different crystals embedded in the glass matrix, as shown in Figure 6. The specific size of each crystal is observed as follows: NaF in range 150–200 nm, CaF<sub>2</sub> in range 50–100 nm, and BaF<sub>2</sub> in a range 20–30 nm. In Figure S15, we present a typical TEM image of a selected area from the pristine opal glass slab (the top air smooth surface is at the bottom of the image), with energy-dispersive X-ray spectroscopy (EDS) mappings of Na and F from the same region: we can observe large crystals of NaF, relatively close to the surface (about 500 nm). Note that this selected size-limited area is probably not representative of the whole sample, since usually we do not observe crystals under the smooth surface in a zone of approximately the same thickness as that observed by SEM (about 9 μm). As evidenced in Figure 3 from the ToF-SIMS analysis, the profiles reveal some clear trends for Na, K, Al, Ca,

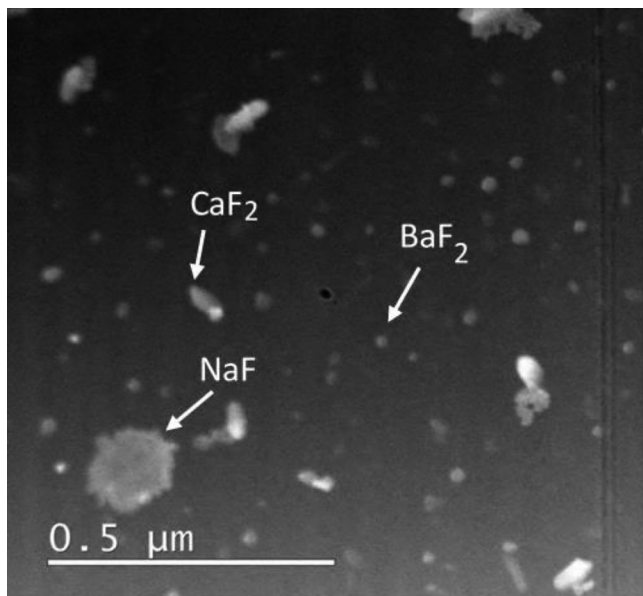


**FIGURE 6** Transmission electron microscopy (TEM) image of a selected area of the pristine opal glass slab.

and Ba, both on large and small scales (15  $\mu\text{m}$  vs. 1.5  $\mu\text{m}$ ). In order to confirm these trends, we performed composition profiles using TEM-EDS. Figure 7 gives the profiles for Na, Ba, and Ca (Figure 7A) and for Si and Al (Figure 7B). As for ToF-SIMS, we observe a layer enriched in Na, Ba, and Ca under the smooth surface of the sample, but the decrease of the concentration is not the same for these elements: the layer is about 4  $\mu\text{m}$  thick for Na, 3  $\mu\text{m}$  for Ca, and 1  $\mu\text{m}$  for Ba. We observe a peak of sodium near the surface: it can be expected that the application of a double protective layer of palladium and platinum can favor the movement toward the surface of certain mobile elements, such as Na. Note that the elemental distribution among the first 200 nm does not show clear trends similar to those observed in ToF-SIMS. Finally, contrary to the ToF-SIMS results, the profile for Si reveals a small depleted zone at the extreme surface (about 200 nm) then an enrichment followed by a slow decrease down to about 4.5  $\mu\text{m}$ .

## 2.2 | Chemical durability of opal glass in acidic medium

### 2.2.1 | Alteration rate derived from the behavior of the bulk material

In our experiment, powder and monolith were altered together, and the monolith was retrieved after 231 days for analysis. The glass powder represents 97% of the glass surface exposed to the acidic solution. Thus the dissolution rate calculated from the concentrations of glass

elements released into the solution mainly corresponds to the behavior of powder rather than that of the slab. According to Figure 8, the alteration can be described as an initial parabolic release of elements in solution within the first tens of days followed by a linear release with time. As expected, the most released element was sodium with a diffusion coefficient calculated from Equation (5)  $D_{\text{Na}} = 6.1 \times 10^{-21} \text{ m}^2 \text{ s}^{-1}$  up to 28 days of alteration. After a month of alteration, the equivalent thickness (ETH) of sodium stopped being clearly linear with the square root of time but showed a direct linear dependency toward time meaning that the rate of hydrolysis was very close to the rate of interdiffusion.<sup>19</sup> Note that the markers of Ca have intentionally been made unobtrusive in Figure 8 as this element was very much subjected to lab contamination resulting in noisy analytical data and unusable rate calculations. But the behavior of calcium is expected to closely resemble the one of barium as observed from the ToF-SIMS data acquired after 231 days of alteration shown in Figure 10.

Overall the predominant leaching mechanism remained the hydrolysis of the glassy network after 28 days. No trend variation was observed all along the 3 years during which the experiment was carried out. The hydrolysis rate was calculated from Equation (4) yielding  $r_{\text{Si}}(t) = 2.6 \times 10^{-3} \text{ g m}^{-2} \text{ d}^{-1}$ .

### 2.2.2 | Remaining alteration layer of the bulk material

After 1096 days (3 years) of alteration, the ETH values calculated from Equations (1) to (3) for network-forming elements Si and Al are the lowest, as expected from their structural role in the glass, with  $\text{ETH}_{\text{geo}} = 1.20 \pm 0.04 \mu\text{m}$ , quickly followed by ETH of Ba and K and capped by Na with  $\text{ETH}_{\text{geo}} = 1.87 \pm 0.06 \mu\text{m}$ . The values were calculated considering a geometrical approximation of the glass powder's surface as explained in subsection II C and Equation (1). To figure out the impact of the surface measurement hypothesis on the calculated ETH values, the glass surface was also measured by Brunauer-Emmett-Teller (BET) method supplying a surfaces' ratio  $S_{\text{BET}}/S_{\text{geo}}$  of 1.83, which is slightly lower than the  $2.5 \pm 0.2$  value typically given as a reference and showed a closest agreement between geometrical and BET methods than usually found in the literature.<sup>20</sup> From the final picture given by ETH calculations presented in Figure 8, a remaining alteration layer depleted in sodium of  $0.67 \pm 0.1 \mu\text{m}$  according to the geometrical approximation of the glass surface and  $0.37 \pm 0.05 \mu\text{m}$  from the BET measurements should be observed. The remaining alteration layer is estimated by subtracting the ETH of Si, which represents the fully

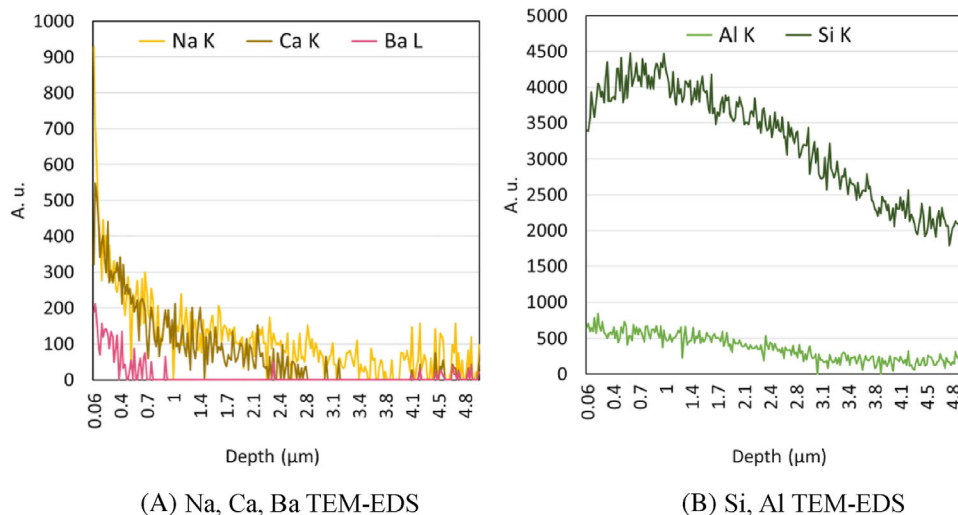


FIGURE 7 Energy-dispersive X-ray spectroscopy (EDS) profiles obtained from the analysis of the smooth surface of a pristine opal crystallized glass plate under transmission electron microscopy (TEM). The vertical axis scale is given in arbitrary units.

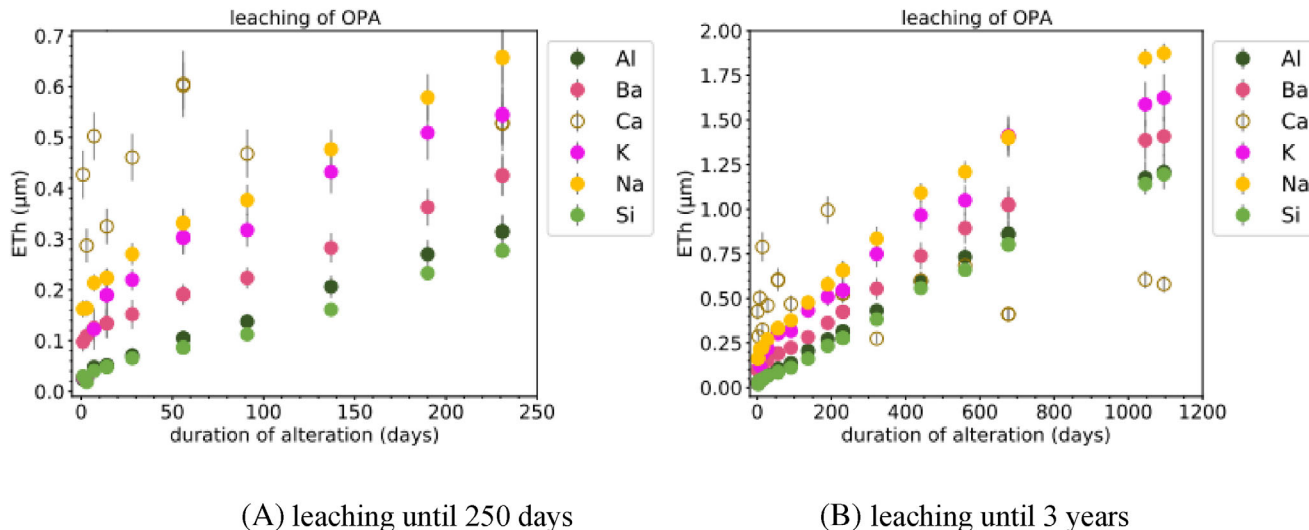


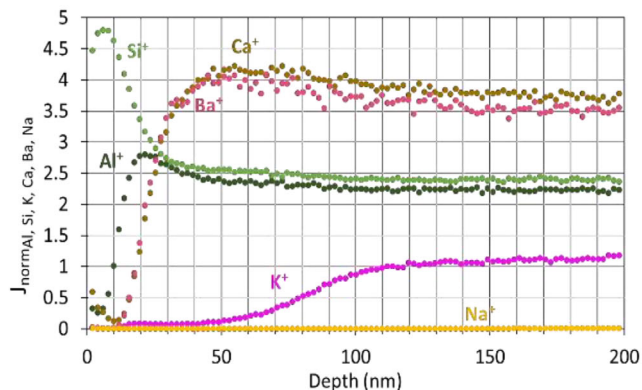
FIGURE 8 Equivalent thickness (ETh) calculations from inductively coupled plasma atomic emission spectroscopy (ICP-AES) data and geometric approximation of the glass surface of the main elements through time for opal glass powder at 70°C, pH = 2.4.

dissolved glass, to the ETh of Na, the most leached out element.

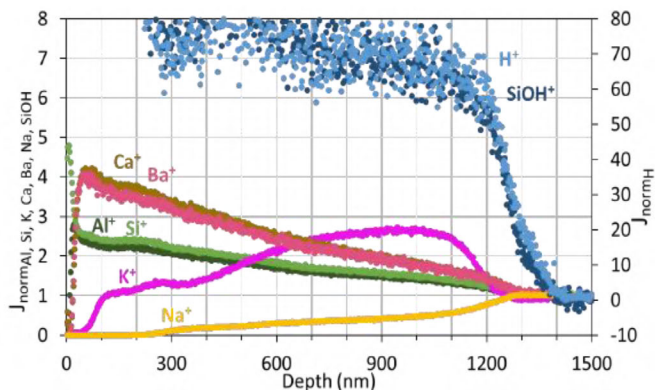
### 2.2.3 | Remaining alteration layer of the slab

According to SEM mapping and ToF-SIMS profiles conducted before alteration on identical samples (Figures 2 and 3), the top first 5  $\mu\text{m}$  of the smooth face does not contain F nor crystals detectable through SEM (diameters superior to 50 nm). In other words, the glass discussed hereafter has a vitreous aspect with soda-lime-like composition. After 231 days of alteration the glass slab was

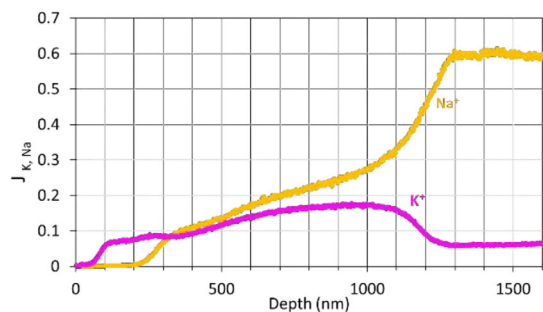
removed from the reactor. Surface characterizations were then conducted on the smooth face of the altered slab showing a total alteration depth of 1.40  $\mu\text{m}$  estimated thanks to the ToF-SIMS profiles of  $\text{H}^+$  and  $\text{SiOH}^+$  as displayed in Figure 9B and  $1.25 \pm 0.022 \mu\text{m}$  according to the measurement conducted by spectroscopic ellipsometry presented in Figure 10. ToF-SIMS and spectroscopic ellipsometry are in good agreement although their probing area is very different. ToF-SIMS was carried out on a  $50 \times 50 \mu\text{m}^2$  zone whereas spectroscopic ellipsometry was run on a  $\approx 0.5 \text{ cm}^2$  area, probing a much larger area and yielding a very reliable average value of the global alteration of the smooth slab's face. The remaining



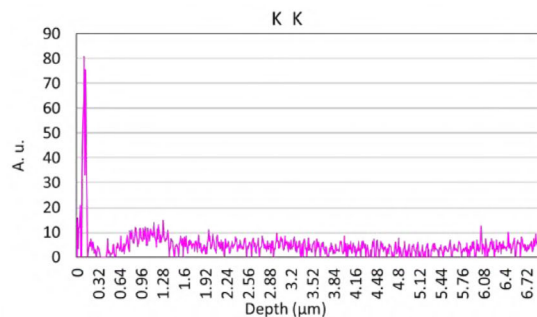
(A) ToF-SIMS profiles until 200 nm



(B) ToF-SIMS profiles until 1.5 μm



(C) ToF-SIMS profiles of Na and K until 1.5 μm



(D) TEM-EDS K

**FIGURE 9** (A–C) Time of flight secondary ion mass spectroscopy (ToF-SIMS) profiles obtained from the analysis of the smooth face of a slab from an opal crystallized glass plate after 231 days of alteration at 70°C and pH = 2.4. The ions displayed represent the species detected by the mass spectrometer after sputtering. The signals are normalized to the total intensity and to the pristine glass for the plots (A, B). (D) Transmission electron microscopy (TEM)–energy-dispersive X-ray spectroscopy (EDS) profile of K (K-spectral line) obtained from opal glass plate slab smooth surface altered 231 days at 70°C in acetic acid 4 vol% (pH = 2.4).

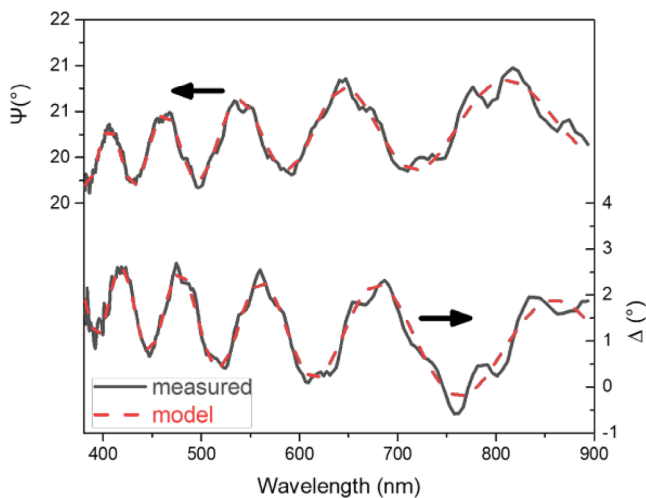


**FIGURE 10** Experimental ellipsometric spectra (in  $\Psi$  and  $\Delta$ ) of opal crystallized glass plate altered 231 days at 70°C and pH = 2.4, measured at room relative humidity. The dashed lines are fittings to experimental data.

alteration layer is mainly depleted in sodium, which can only be explained by a dominant ion-exchange/interdiffusion mechanism, as typically observed in silicate glasses altered in acidic solution.<sup>21,22</sup> The very weak depths depleted in Al, Ca, and Ba are better shown in the detailed plot shown in Figure 9A. A highly similar behavior is observed for earth-alkali Ca and Ba, both exhibiting a 50 nm depleted area at the surface followed by a swift increase and then a slowly decreasing plateau. This plateau could correspond to the initial level of Ca and Ba present in this region of the glass, although the normalized intensity remain above 1, because the profiles collected before alteration (Figure 3) clearly show a continual decrease of Ca and Ba signals in the first 5 μm of the pristine glass. As a matter of fact, the profiles displayed in Figure 9 were normalized to a single value averaged from the nonhydrated segment of the sample analyzed, which explains the apparent enriched area in Ca and Ba both as an artifact from the normalization and the heterogeneity of distribution depthwise of these elements



prior to alteration. Although very consistent in their behavior throughout ToF-SIMS and SEM observations so far, Si and Al exhibit different distributions in the outermost 20 nm of the 231-days-altered glass surface which appears depleted in Al leaving behind an Si-rich and highly hydrated surface layer. The profile obtained for K shows a small area about 100 nm width near the surface fully depleted and followed by a bump spreading across 1.1  $\mu\text{m}$  with normalized intensities above 1 before decreasing to a stable level of intensity corresponding to nonhydrated and thus unaltered glass. The same variations were noticed through TEM-EDS analysis as shown in Figure 9D excluding a simple matrix effect artifact from the ToF-SIMS profile. The peak near the extreme surface (0–0.3  $\mu\text{m}$ ) is probably due to the presence of the Pt-Pd protection layers deposition which could promote the migration of elements. In Figure 9A, plot featuring the profiles of Na and K only is given and the severely Na depleted zones appeared to be the locations where K is retained (Figure 9C). The opposite reciprocity of the distribution of these elements in the remaining altered layer let us think that K plays a role in compensating the absence of Na during the alteration process and raises the question of the origin of the K accumulated in the alteration layer. The origin of K can be twofold: (i) from the glass, through the internal migration of potassium contained in the underlying pristine glassy matrix toward the solution through the alteration layer fostered by exchanges with solution's protons that have penetrated in the glass and (ii) K from the container or the solution, unwillingly present, often brought by pH electrode or other kinds of contamination resulting in external additions of K to the alteration medium. In the glass alteration literature, external addition of KCl salt to the alteration solution is reported to impact glass dissolution rate through incorporation of K in the alteration layer.<sup>23,24</sup> In these studies, the lowest concentrations of K to obtain a sensitive effect are at least a hundred times greater than the concentration reported here. Thus, it is likely that the K observed in the alteration layer in Figure 9 is of endogenous origin, that is not diffusing from the alteration solution into the glass sample under alteration but from the internal layers of the glass toward the external layers.

#### 2.2.4 | TEM-EDS analysis of the altered slab

In-depth monitoring of the sodium content seems to be a good indicator for the identification of the alteration layer. We observe a depletion of Na in a region about 1.5  $\mu\text{m}$  thick below the smooth surface of the altered opal glass, as shown in Figure 11A. This result is consistent with those from ToF-SIMS and spectroscopic ellipsometry, which pro-

posed an alteration layer thickness ranging from 1.25 to 1.40  $\mu\text{m}$ . The Na content profile is presented in Figure 11B: it displayed a depleted zone about 1.5  $\mu\text{m}$  thick below the surface, then an enrichment in sodium, which content then decreases slowly to a depth of about 5  $\mu\text{m}$  as already observed on the pristine glass by ToF-SIMS (Figure 3A). It is assumed that the alteration layer corresponds to this layer 1.5  $\mu\text{m}$  thick depleted in Na.

We also realized EDS-TEM profiles for the other elements, to compare them to those obtained by ToF-SIMS and presented in Figure 9. For Ca and Ba, we got almost the same results (see Figure S16A,B): for Ca, the profile is the same, with a narrow depletion layer (about 50 nm thick) at the extreme surface, then a swift increase followed deeper by a slowly decreasing plateau. For Ba, the extreme surface depleted layer is not clearly evidenced but the following zones are present.

For Si and Al, we obtained roughly the same results as those presented for ToF-SIMS (Figure 9A): the narrow region where Al and Si exhibit different behavior is probably more about 40 nm thick just below the extreme surface (see Figure S17). The swift increases of both concentrations are actually shifted, with the Si profile increasing about 20 nm before that of Al, and both profiles reached their maximum point over a region of about 40 nm thick.

#### 2.2.5 | Alteration rate of the slab

In the same reactor, opal crystallized glass plates were altered under two different forms: powder and slab. The remaining alteration layer has been carefully characterized in both cases but only the kinetics of the powder is available. Applying the kinetics obtained on the powder to try to match the final picture given by characterizations of the slab after 231 days of alteration is possible by taking into account the shape factor described by Fournier et al.<sup>20</sup> Theoretically the ratio of alteration rates obtained on powder (with geometrical approximation of the surface) versus slab is

$$F_s = \frac{R_{0 \text{ powder}}}{R_{0 \text{ slab}}} = 1.3 \pm 0.3$$

which can also be expressed as

$$F_s = \frac{E_{\text{Th}x \text{ powder}} - E_{\text{ThSi}} \text{ powder}}{E_{\text{Th}x \text{ slab}}} = 1.3 \pm 0.3$$

where  $x$  is a glass constituting element measured in solution and  $E_{\text{Th}x \text{ slab}}$  is the depth depleted in element  $x$  from the ToF-SIMS corresponding profile. The shape factor obtained for the elements depleted after 231 days are given in Table 3. The calculated  $F_s$  values do not range into the

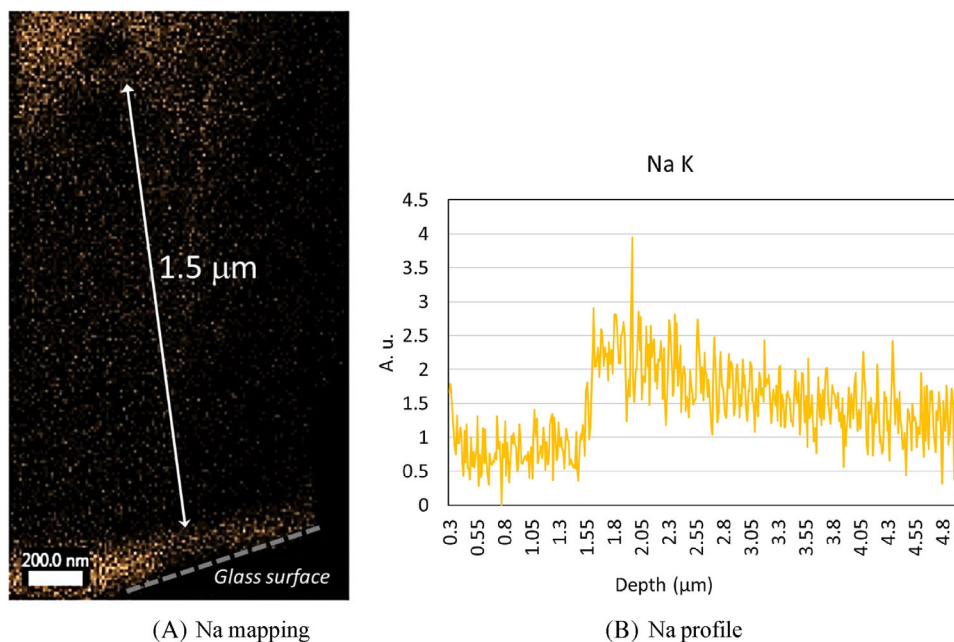


**FIGURE 11** (A) Energy-dispersive X-ray spectroscopy (EDS) mapping of Na in a selected area of the 231-days-altered opal glass. The surface of the altered glass slab is indicated by the dotted line at the bottom of the picture. (B) EDS profile of Na from the smooth surface of the altered opal glass. The horizontal axis scale is in micrometers.

**TABLE 3** Shape factor calculated from solution analysis and time of flight secondary ion mass spectroscopy (ToF-SIMS) profiles for Na, Al, Ba, Ca, and K in opal crystallized glass plate after 231 days of alteration at 70°C and pH = 2.4.

Element	$F_s$
Na	0.27
K	0.21
Al	1.89
Ba	3.16
Ca	5.34

limits determined by Fournier et al. displaying great discrepancies between the powder and slab alteration rates that cannot be only imputed to the shape of the glass. Other conceivable reasons for such differences between glass powder and slab are multiple and intertwined. First, the microstructure of slab and monolith differs. The glass slab exhibits a fully vitreous outer layer. Conversely, the glass powder is predominantly composed of grains with a high density of 50–200 nm crystals embedded in a crystal matrix. Second, as a result of microstructural differences, the chemical composition of the two materials is not strictly equivalent. Although it is not possible to accurately analyze the composition of the glassy phase in the crystallized region (the great magnification required to hit in between crystals caused the well-known migration of alkali from the glassy matrix under the electron beam, altering the targeted composition), one can expect differ-

ences based on the presence of alkali and alkaline earth in the crystals. These differences could explain why the slab's alteration is dominated by interdiffusion after 231 days in acetic acid 4% (v/v) at 70°C whereas the alteration kinetics of the powder show the preponderating role of hydrolysis under the very same conditions.

### 2.2.6 | Structure of the altered bulk glass

After 969 days of alteration, a small amount of powder was sampled from the reactor and analyzed by MAS NMR spectroscopy again to investigate structural changes of sodium and fluorine caused by the alteration in acetic acid 4% (v/v). The spectra collected after alteration for  $^{19}\text{F}$  and  $^{23}\text{Na}$  nuclei are presented in Figure 12. All the  $^{19}\text{F}$  spectra given in Figure 12A,B were acquired with 256 s recycling delay to allow full comparison of the data on pristine and altered glass including quantification. As shown by the overlap of the spectra, the results obtained are fairly the same before and after alteration, validating a congruent dissolution mechanism of glass and crystals simultaneously. Regarding sodium, the quantification of the crystalline phases from the  $^{23}\text{Na}$  MAS NMR spectrum after alteration (Figure 12C) yielded 43% of Na distributed in the NaF crystals and 57% in the glassy matrix which remained very close to the proportions calculated before alteration (44% and 56%, respectively). Nonetheless, a slight decrease of the width of NaF line after alteration can

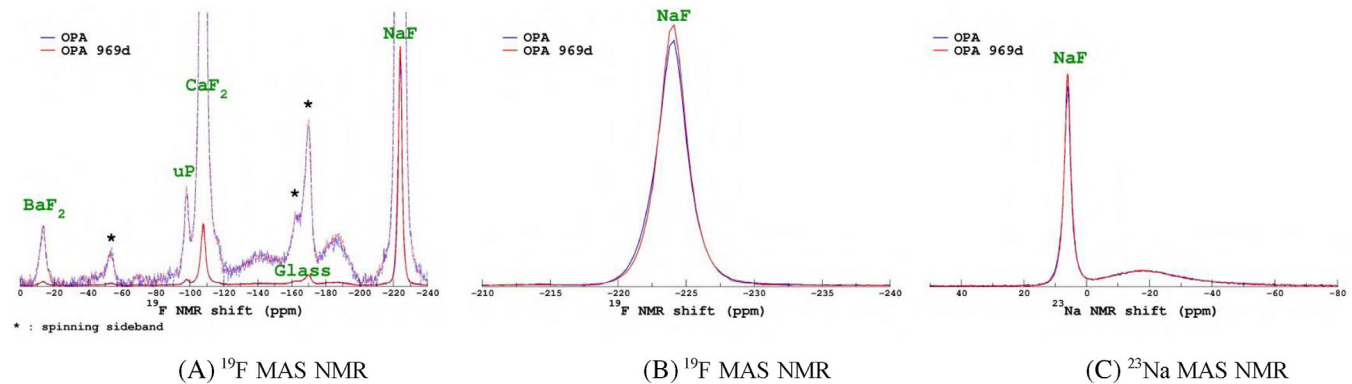


**FIGURE 12** (A) Experimental magic-angle spinning nuclear magnetic resonance (MAS NMR)  $^{19}\text{F}$  spectra obtained from pristine (OPA) and altered for 969 days (OPA 969d) in acetic acid 4% (v/v) at  $70^\circ\text{C}$  opal crystal glass powder, the dashed lines are amplifications of the spectra shown with solid lines and (B) exhibits a focus on the line of NaF before (OPA) and after alteration (OPA 969d). The same line of NaF seen from  $^{23}\text{Na}$  MAS NMR is displayed in figure C. All spectra were obtained from the same pristine and altered 969 days opal glass powders at 25 kHz and 11.72 T.

be noticed regarding this compound probed by  $^{23}\text{Na}$  and  $^{19}\text{F}$  MAS NMR (Figure 12A,C, respectively). This feature indicates the mild reduction of the quadrupolar coupling constant ( $C_q$ ), probably reflecting the presence of protons around the nucleus that decreases the  $C_q$  value and as a consequence the distribution of NMR lines.<sup>25</sup>

A significantly higher chemical resistance from one of the crystalline phases is unlikely. Indeed, it would necessarily conduct to a notably different ratio of distribution before and after alteration. Therefore, this result is consistent with a mechanism of alteration mainly driven by hydrolysis of the silicate glassy matrix that controls the behavior of the whole materials, leading to a very slight preferential release of sodium, as expected from a fully vitreous soda-lime glass.

### 3 | CONCLUSION

Opal crystallized glass plates appear very different at various scales with each scale of analysis bringing up a unique level of information. In the pristine glass plate, we can visually determine at a macroscopic scale a thin vitreous region and a thick opaque region in the width of plate. From a microscopic point of view, most of the material is homogeneous except for variations of elements distribution close to the top and bottom surfaces of the plate. At a micro to nanometric scale, the glassy matrix is riddled with three different types of crystals making it a composite yet compact bulk material. These observations outline the necessity to study this material from different aspects. First, the bulk material, under the form of powder, gives an overview of the structure and chemical durability. Structural information regarding the crystalline phases and evidences of fluorine in the glassy matrix were

obtained. As a result, no evolution was noticed along the 3 years of alteration, which is driven by hydrolysis of silicate network that controls the behavior of the whole matrices. A slab comprising the top and bottom faces of the plate shows a very different microstructure with no crystals near the surface and enrichment in Na, Ba, and Ca correlated with a depletion in F in the top 10  $\mu\text{m}$  near the top smooth face. After 231 days of alteration, evidences of a higher interdiffusion than hydrolysis rate of alteration were observed from the micrometer-sized remaining alteration layer. Evidently, the surface and bulk of a single plate do not have the same kinetics nor mechanisms of alteration as the bulk material but overall the great durability of this opal crystallized glass under harsh alteration conditions such as acetic acid 4% (v/v), at  $70^\circ\text{C}$  for very long periods of time can be outlined. Especially the alteration of the bulk which is governed by the hydrolysis of the material, evolving at a constant, characterized, and predictable rate at the same order of magnitude as resistant vitreous silicate glasses reported in the literature.<sup>1,22,26</sup>

In perspective of this work, additional experiments could be conducted at lower temperatures to evaluate, through a model such as the one proposed for Pb in the lead crystal glass,<sup>27</sup> the release of elements like Ba or F by opal glass under conditions of dishware usage.

### 4 | METHODS

#### 4.1 | Glass preparation

Opal glass plates were received directly from the manufacturer. Rectangular glass slabs were cut out from each item and the raw edges were polished to 1  $\mu\text{m}$  (roughness of the order of a few nm), no annealing step was performed.

Slabs were cleaned with acetone and ethanol before use. This is an important step because we observed a deposit on the surface of the glass plates at reception. The deposit is composed of sodium carbonates. It is likely due to a reaction with air moisture. Plates were stored 4 weeks at room temperature and humidity before shipping to our lab.

Glass powder with grain diameters ranging from 63 to 125  $\mu\text{m}$  was prepared following a classical procedure based on crushing, sieving and cleaning in acetone and ethanol to remove fine particles. Then BET method<sup>28</sup> on a Micromeritics ASAP 2010 instrument with krypton gas was performed on the mentioned powder and the specific surface area of the powder was measured. Finally, the ground powders were analyzed by Filab using inductively coupled plasma atomic emission spectroscopy (ICP-AES) to determine the molar composition of the bulk glass which was then normalized and converted to weight percent.

## 4.2 | NMR spectroscopy

MAS NMR data were collected on a Bruker Avance Neo 500WB spectrometer operating at a magnetic field of 11.72 T. A commercial Bruker CPMAS 2.5 mm (outer diameter of the  $\text{ZrO}_2$  rotors) was used at a spinning frequency of 25 kHz. A recycle delay of 32 s and 256 s was used for  $^{23}\text{Na}$  and  $^{19}\text{F}$ , respectively. The NMR shifts were referenced to external 1 M aqueous NaCl ( $^{23}\text{Na}$ , 0 ppm), 1.0 M aqueous  $\text{Al}(\text{NO}_3)_3$  (0 ppm), and using the  $\text{CaF}_2$  ( $^{19}\text{F}$  108 ppm) peak.  $^{23}\text{Na}$  and  $^{27}\text{Al}$  were acquired using a single sort pulse excitation (1  $\mu\text{s}$ ) whereas, to cancel probe background signal,  $^{19}\text{F}$  was acquired using rotor-synchronized Hahn Echo sequence (90– $\tau$ –180– $\tau$  acquisition, with  $\tau$  being equal to a single rotor period). Data were processed and fitted using an in-house package (T. Charpentier). For  $^{19}\text{F}$  MAS NMR, peaks and spinning sidebands were fitted using a mixture of Gaussian and Lorentzian. For  $^{23}\text{Na}$ , NaF peaks (centerband and spinning sidebands) were simulated using a single Gaussian line shapes; the broad glass peak was simply simulated using two Gaussians (to account for the NMR parameter distribution, see Soleilhavoup et al.<sup>29</sup> In both cases ( $^{19}\text{F}$  and  $^{23}\text{Na}$ ), the aim of the fit was to quantify each phase contribution.

## 4.3 | Leaching experiments

Long-term alteration in static mode was performed in perfluoroalkoxy alkane (PFA) reactors at  $70 \pm 3^\circ\text{C}$  in 4% (v/v) acetic acid solution, which translates to a pH of  $2.4 \pm 0.1$ . About 800 mg of 63–125  $\mu\text{m}$  particle size glass powder and a single glass slab were added to a large volume of acetic acid.

The precise quantities of solution and glass were carefully measured and the resulting glass-surface-area-to-solution-volume ratio  $\text{SA}/V$  was calculated. This experiment being designed for long-term alteration, it is likely to use the geometric approximation described in Equation (1), rather than the BET measurements. As demonstrated by Fournier et al.,<sup>30</sup> BET is very sensitive to nanoscale rugosity, which tends to increase the glass surface area significantly and is not so accurate after the first stage of alteration. Both methods of calculation are used in this paper, leading to  $\text{SA}/V$  initial values of  $50.5 \text{ m}^{-1}$  using the geometrical approximation given in Equation (1) and  $92.5 \text{ m}^{-1}$  with the classical BET approach. The difference between these two values is discussed with the leaching results. Since there was no stirring, the glass powder lied at the bottom of the reactor and the glass slab was elevated by a PFA stand to avoid contact between the slab and the powder.

$$\frac{\text{SA}_{\text{geo}}}{V} = \frac{3 \cdot m_{\text{glass}}}{V_{\text{sol}} \cdot \rho \cdot R_{\text{mean}}} \quad (1)$$

where  $\text{SA}_{\text{geo}}/V$  is the glass-surface-area-to-solution-volume-ratio determined with the geometric approximation ( $\text{m}^{-1}$ ),  $V_{\text{sol}}$  is the volume of solution in the experiment ( $\text{m}^3$ ),  $m_{\text{glass}}$  is the mass of glass in the experiment (g),  $\rho$  is the density of the glass ( $\text{g m}^{-3}$ ), and  $R_{\text{mean}}$  is the mean radius of glass particles in the experiment (m).

The reactor was tightly closed and Teflon ribbon was applied on the screwing neck to make the reactor airtight. Then, the reactor was placed in a larger vessel, filled with some water, to ensure homogeneous temperature and avoid evaporation in the primary reactor. The alteration solution was regularly sampled from the reactor (15 times in total). Each sample consists of removing 1 mL of solution using a syringe and then acidifying it with 0.5N ultrapure  $\text{HNO}_3$  for analysis by ICP-AES. The solution withdrawal generated by the samplings is considered by recalculating the glass-surface-area-to-solution-volume-ratio after each sampling. The normalized mass loss for each element of each sample was calculated using Equation (2).

$$\text{NL}_{\text{geo}, i} = \frac{C(i)_t}{(\text{SA}_{\text{geo}}/V)_t \cdot x_i} \quad (2)$$

where  $\text{NL}_{\text{geo}, i}$  is the normalized mass loss of glass determined from element  $i$  after  $t$  days of alteration ( $\text{g m}^{-2} \text{ d}^{-1}$ ),  $C(i)_t$  is the concentration of element  $i$  in solution after  $t$  days of alteration ( $\text{g m}^{-3}$ ),  $\text{SA}_{\text{geo}}/V_t$  is the glass-surface-area-to-solution-volume-ratio determined with the geometric approximation after  $t$  days of alteration ( $\text{m}^{-1}$ ), and  $x_i$  is the mass fraction of element  $i$  in the pristine glass.



These normalized losses per element can be translated to ETh of glass altered thanks to Equation (3) and enable the calculation of alteration rates through partial derivation with respect to time given in Equation (4).

$$\text{ETh}_{\text{geo}, i} = \frac{\text{NL}_{\text{geo}, i}}{\rho} \quad (3)$$

where  $\text{ETh}_{\text{geo}, i}$  is the equivalent thickness of glass altered for element  $i$  after  $t$  days of alteration ( $\mu\text{m}$ ),  $\text{NL}_{\text{geo}, i}$  is the normalized losses of element  $i$  in solution after  $t$  days of alteration ( $\text{g m}^{-2} \text{d}^{-1}$ ), and  $\rho$  is the pristine glass density ( $\text{g m}^{-3}$ ).

$$r_i(t) = \frac{\partial \text{NL}_{\text{geo}, i}}{\partial t} \quad (4)$$

where  $r_i(t)$  is the releasing rate of an element  $i$  for a given time of alteration ( $\text{g m}^{-2} \text{d}^{-1}$ ) and  $\text{NL}_{\text{geo}, i}$  is the normalized losses of element  $i$  in solution after  $t$  days of alteration ( $\text{g m}^{-2} \text{d}^{-1}$ ).

The diffusion coefficients for species with diffusion behavior were calculated using Equation (5)

$$D_i = \pi \left( \frac{r_i(t)}{2\rho} \right) \quad (5)$$

where  $D_i$  is the diffusion coefficient of an element  $i$  for a given time of alteration ( $\text{m}^2 \text{s}^{-1}$ ),  $r_i(t)$  is the partial derivative of normalized losses of element  $i$  with respect to time ( $\text{g m}^{-2} \text{s}^{-0.5}$ ), and  $\rho$  is the pristine glass density ( $\text{g m}^{-3}$ ).

Correction factors to ensure data consistency throughout the five different campaigns of analysis were computed. For the first and/or last sampling times of an analytical batch, two measurements of the concentration were performed allowing for the calculation of a correction factor  $f$ , as broke down in Equation (6). This correction factor has then been applied to all the values in the analytical batch using Equation (7). This adjustment method was iterated for each analytical batch and the values displayed in the plots of this paper are derived from the adjusted concentrations.

$$f_{\text{corr}, j} = \frac{C(i)_{t, j-1} - C(i)_{t, j}}{C(i)_{t, j}} \quad (6)$$

where  $f_{\text{corr}, j}$  is the correction factor,  $C(i)_{t, j-1}$  is the concentration of element  $i$  in solution after  $t$  days of alteration obtained from analytical batch  $j-1$  ( $\text{g m}^{-3}$ ), and  $C(i)_{t, j}$  is the concentration of element  $i$  in solution after  $t$  days of alteration obtained from analytical batch  $j$  ( $\text{g m}^{-3}$ ).

$$C(i)_{\text{corr}, j} = C(i)_{t, j} \cdot (1 + f_{\text{corr}, j}) \quad (7)$$

where  $C(i)_{\text{corr}, t, j}$  is the adjusted concentration of element  $i$  in solution from analytical batch  $j$  after  $t$  days of alteration based on the values obtained from analytical batch  $j-1$  ( $\text{g m}^{-3}$ ),  $C(i)_{t, j-1}$  is the concentration of element  $i$  in solution after  $t$  days of alteration obtained from analytical batch  $j-1$  ( $\text{g m}^{-3}$ ), and  $C(i)_{t, j}$  is the concentration of element  $i$  in solution after  $t$  days of alteration obtained from analytical batch  $j$  ( $\text{g m}^{-3}$ ).

After 231 days of alteration the glass slab was removed from the reactors, washed with deionized water and slowly dried to be characterized by ToF-SIMS and spectroscopic ellipsometry. The powder, which was responsible for more than 97% of elemental release in solution, remained in the reactor and samplings were carried on until 1096 days, which corresponds to exactly 3 years of alteration.

#### 4.4 | ToF-SIMS

Depth profiles were analyzed on the smooth face of the pristine and altered glass slabs by ToF-SIMS with an IONTOF TOF 5 instrument at Tescan Analytics (Fuveau, France) using  $\text{O}^{2+}$  sputtering and  $\text{Bi}^{+}$  analyzing beams scanning a surface area of  $50 \times 50 \mu\text{m}^2$ . Oxygen beam was tuned at 1 keV and 130 nA and only positive mode was used excluding the analysis of fluorine. The depth of the craters was measured after the analyses, and profiles were calculated assuming that the sputtering rate was constant. First of all, at each mass analysis, the intensity of each element was individually normalized to the total intensity accounting for all the ions collected to rectify any fluctuation from the ion source, as shown in Equation (8). Then, the profiles of interest were normalized to the mean value obtained in the pristine glass with Equation (9) to cut off the signal of the pristine glass and evaluate the relative behavior of each element in the altered glass. All elements are thus normalized to 1 in the pristine glass. Finally, the data have been normalized compared to pristine glass and Si using Equation (10), since the leaching rate of Si was the lowest and thus considered as the least mobile element in this glass after 231 days of alteration.

$$J_i = \frac{A_i}{A_{\text{tot}}} \quad (8)$$

where  $J_i$  is the intensity of element  $i$  normalized to the total count of ions,  $A_i$  is the intensity of element  $i$ , and  $A_{\text{tot}}$  is the total intensity collected on the mass spectrometer.

$$J_{\text{norm}, i} = \frac{J_i}{\frac{I}{n_{\text{sup}} - n_{\text{inf}}} \sum n_{\text{inf}}^{n_{\text{sup}}} J_i} \quad (9)$$

where  $J_{\text{norm},i}$  is the intensity of element  $i$  normalized to the pristine glass,  $J_i$  is the intensity of element  $i$  normalized to the total count of ions,  $n_{\text{inf}}$  is corresponding to a point in the pristine glass, and  $n_{\text{sup}}$  is corresponding to the maximum profile depth.

$$J_{\text{norm,Si}} = \frac{\frac{J_i}{J_{\text{Si}}}}{\frac{I}{n_{\text{sup}} - n_{\text{inf}}} \sum n_{\text{inf}} \frac{J_i}{J_{\text{Si}}}} \quad (10)$$

where  $J_{\text{norm,Si}}$  is the intensity of element  $i$  normalized to the pristine glass and Si,  $J_i$  is the intensity of element  $i$  normalized to the total count of ions,  $J_{\text{Si}}$  is the intensity of Si normalized to the total count of ions,  $n_{\text{inf}}$  is corresponding to a point in the pristine glass, and  $n_{\text{sup}}$  is corresponding to the maximum profile depth.

For initial glass constituting elements (i.e., Si, Al, Na, Ba, and Ca), the thickness of glass depleted for each element has been estimated by collecting the depth corresponding their maximal normalized intensity  $J_{\text{norm},i}$ . The hydrated depth of the sample has been determined by considering the depth of  $\text{H}^+$  and  $\text{SiOH}^+$  species when the normalized intensity  $J_{\text{norm}}$  reaches 1. Please note that the ionic form exhibited in the figure's legend or in the text do not represent the ionization of the elements in the glass sample but the species detected by the secondary ion mass spectrometer after sputtering.

#### 4.5 | Spectroscopic ellipsometry

The glass slab altered 231 days has been roughen with SiC grinding paper on one large side to prevent the backside reflection during the ellipsometry measurements. The sample was then thoroughly cleaned, and the analysis was carried out at the Pennsylvania State University in the Department of Chemical Engineering and Materials Research Institute. Detailed procedures and explanations are available in Ngo et al.<sup>31</sup> In ellipsometry, information about the sample under the study is obtained by fitting measured ellipsometric spectra to an optical model. The current study used a rotating compensator spectroscopic ellipsometer (J.A. Woollam Co. Alpha-SE) that had a wavelength range of 381–893 nm. The incident angle of light used in the study was 70°. The measurements were carried out at room relative humidity (40%–50%). Pristine glass slab was first measured and analyzed, and the obtained optical properties were used as the substrate in the optical model of the altered sample. The spectroscopic ellipsometry (SE) spectra fittings in this study were performed using the CompleteEASE software package. The optical model for the altered glass sample included multiple sublayers for the alteration layer on top of the substrate (pristine glass). Each sublayer consisted of a glass and a void (porosity)

ity) component, and the Bruggeman effective medium approximation (EMA) was used in calculating the optical response of each sublayer in the alteration layer.<sup>32</sup> In the SE analysis, each sublayer was assumed to be optically isotropic and the boundaries between them to be parallel. The pore sizes were considered to be small in comparison to the wavelength of the incident light. This assumption was required to validate the use of the EMA. It was also assumed that the optical properties of the solid part of the leached layer are the same as those of the studied pristine glass. This assumption was made due to the difficulty in accurately determining the refractive index of the solid part and the fraction of porosity of each sublayer in the alteration layer.

#### 4.6 | Scanning electron microscopy

The morphology of the pristine slab and powder and the altered powder were examined by field emission gun (FEG)-SEM using a Zeiss Supra 55 at 15 kV (probe current about 1 nA). To allow precise mapping, the samples were embedded in an epoxy resin and polished before coating with a 15 nm carbon layer for electronic conduction. The determination of the chemical distribution of the different phases within the samples was obtained from EDS analyses on plane polished samples with a Bruker AXS X-FlashDetector 4010 system. Data collection and treatment were done with the ESPRIT2.0 software (Bruker™)

#### 4.7 | X-ray diffraction

XRD patterns were collected on a D8 advance diffractometer from Bruker operating at 35 kV and 40 mA, using  $\text{Co-K}\alpha$  radiation (1.79 Å) at an angular step of 0.01° s<sup>-1</sup> between 3.0° and 80.0° (2θ) angles. The EVA software coupled with the ICDD pdf-2 database enabled the identification of the major phases in the materials. Prior to XRD experiments, opal glass samples were crushed and ground in a tungsten ball mill and sifted in a 32 μm sieve. After sieving, samples powders were sprinkled gently in XRD sample holder using a 65 μm sieve. The top layer was removed carefully by cutting the surface with a thin razor blade leading a smooth surface without compaction: such preparation allows to decrease the preferential orientation of particles.

#### 4.8 | Transmission electron microscopy coupled with energy dispersive X-ray spectrometry

Nanoscale characterization was performed by transmission electron microscopy on ultrathin sections. Samples were prepared by focused ion beam (FIB) milling with an

FEI FIB 200 SEM system or with a FEI Hélios NanoLab 650 Dual beam microscope. During FIB preparation, a few nanometers thick layer of carbon was first applied on the samples to make them conductive. Then two few micrometers thick layers of platinum (Pt) and palladium (Pd) were then coated on the surface to protect the samples. Afterward the FIB cuts were carved and thinned using gallium (Ga) ions beam. TEM observations were carried out on a FEI Tecnai F20 microscope equipped with a FEG, a GATAN scanning device (STEM) and a complete set of detectors that allows image acquisition in a range of operating modes (dark field, bright field, and high angle annular dark field) and a spatial resolution of 0.24 nm. The STEM is coupled with a Si(Li) detector (EDAX Sapphire r-TEM): the energy-dispersive X-ray spectrometry capability coupled to the TIA ES Vision software (FEI Inc.) were used to determine the chemical composition of the compounds and phases of interest. During TEM observations and analyses, we had to face and solve two problems: (i) the FIB preparation by ions milling required protection layers and generated implementation of elements inside the studied materials: in all observations we had to consider the implementation of Ga, for example, and slight diffusion of platinum at the extreme surface of the samples; (ii) the opal glasses studied in this work turned out to react strongly under the electron beam: to limit the irradiation damage and to make the analyzes more reliable, sometimes requiring long acquisition times, we sometimes had to limit the accelerating voltage of the electrons in order to limit their energy, and an observation and analysis protocol adapted to each sample had to be implemented in order to obtain reliable information and quality data on the opal glasses studied.

### AUTHOR CONTRIBUTIONS

Pierre Asplanato and Léa Brunswic performed the leaching experiments, Léa Brunswic carried out the MO and SEM observations and all the data curation. Laurent Gautron was responsible for the TEM preparations and observations. Thibault Charpentier performed the NMR studies. Huseyin Kaya and Seong H. Kim took care of the spectroscopic ellipsometry. Frédéric Angeli, Stéphane Gin, and Léa Brunswic supervised the study and worked on the conceptualization, methodology, and original draft. All the authors helped on the paper editing.

### ACKNOWLEDGMENTS

This study was supported by the French Agency for Research (ANR, PRCE program, grant 18-CE08-0025). Prime Verre prepared the glass slabs and glass powders. Elodie Chauvet, Loan Lai, Florian Cousy, and Yves Depuydt from Tescan Analytics performed the Tof-SIMS profiles.

Géraldine Parisot analyzed the solutions by ICP-AES. Filab, France, analyzed the glass composition. Patrick Jolivet is acknowledged for igniting this experimental work. Myriam Duc from the GERS Department of Université Gustave Eiffel, France is acknowledged for her invaluable help and assistance for the X-ray diffraction experiments. Laurent Gautron would like to particularly thank Eric Leroy (ICMPE, Université Paris-Est Créteil, France) for his assistance during the observations and analyzes by transmission electron microscopy.

### CONFLICT OF INTEREST STATEMENT

The authors declare no conflicts of interest.

### DATA AVAILABILITY STATEMENT

The data that support the findings of this study are available from the corresponding author upon reasonable request.

### ORCID

Léa Brunswic  <https://orcid.org/0000-0002-5072-9620>

Frédéric Angeli  <https://orcid.org/0000-0001-5632-7684>

Thibault Charpentier  <https://orcid.org/0000-0002-3034-1389>

Stephane Gin  <https://orcid.org/0000-0002-1950-9195>

Seong H. Kim  <https://orcid.org/0000-0002-8575-7269>

### REFERENCES

1. Stone-Weiss N, Youngman RE, Thorpe R, Smith NJ, Pierce EM, Goel A. An insight into the corrosion of alkali aluminoborosilicate glasses in acidic environments. *Phys Chem Chem Phys*. 2020;22:1881–96.
2. Lee WE, Ojovan MI, Stennett MC, Hyatt NC. Immobilisation of radioactive waste in glasses, glass composite materials and ceramics. *Adv Appl Ceram*. 2006;105:3–12.
3. Majérus O, Lehuédé P, Biron I, Alloteau F, Narayanasamy S, Caurant D. Glass alteration in atmospheric conditions: crossing perspectives from cultural heritage, glass industry, and nuclear waste management. *NPJ Mater Degrad*. 2020;4:27.
4. Mattson SM. Glass-fibers in simulated lung fluid—dissolution behavior and analytical requirements. *Ann Occup Hyg*. 1994;38:857–77.
5. Hench LL. The story of Bioglass®. *J Mater Sci-Mater Med*. 2006;17:967–78.
6. Stefánsson A, Gíslason SR. Chemical weathering of basalts, southwest Iceland: effect of rock crystallinity and secondary minerals on chemical fluxes to the ocean. *Am J Sci*. 2001;301:513–56.
7. Gin S, Beaudoux X, Angéli F, Jégou C, Godon N. Effect of composition on the short-term and long-term dissolution rates of ten borosilicate glasses of increasing complexity from 3 to 30 oxides. *J Non-Cryst Solids*. 2012;358:2559–70.
8. Cagnon B, Daval D, Cabié M, Lemarchand D, Gin S. A comparative study of the dissolution mechanisms of amorphous and crystalline feldspars at acidic pH conditions. *NPJ Mater Degrad*. 2022;6:34.

9. Frankel GS, Vienna JD, Lian J, Guo XL, Gin S, Kim SH, et al. Recent advances in corrosion science applicable to disposal of high-level nuclear waste. *Chem Rev.* 2021;121:12327–83.
10. Frankel GS, Vienna JD, Lian J, Scully JR, Gin S, Ryan JV, et al. A comparative review of the aqueous corrosion of glasses, crystalline ceramics, and metals. *NPJ Mater Degrad.* 2018;2:15.
11. Gin S, Delaye JM, Angeli F, Schuller S. Aqueous alteration of silicate glass: state of knowledge and perspectives. *NPJ Mater Degrad.* 2021;5:42.
12. Thorpe CL, Neeway JJ, Pearce CI, Hand RJ, Fisher AJ, Walling SA, et al. Forty years of durability assessment of nuclear waste glass by standard methods. *NPJ Mater Degrad.* 2021;5:61.
13. Angeli F, Charpentier T, Jollivet P, de Ligny D, Bergler M, Veber A, et al. Effect of thermally induced structural disorder on the chemical durability of international simple glass. *NPJ Mater Degrad.* 2018;2:31.
14. Nicoleau E, Angeli F, Schuller S, Charpentier T, Jollivet P, Moskura M. Rare-earth silicate crystallization in borosilicate glasses: effect on structural and chemical durability properties. *J Non-Cryst Solids.* 2016;438:37–48.
15. Nicoleau E, Schuller S, Angeli F, Charpentier T, Jollivet P, Le Gac A, et al. Phase separation and crystallization effects on the structure and durability of molybdenum borosilicate glass. *J Non-Cryst Solids.* 2015;427:120–33.
16. Chopinet MH, Verità M, Falcone R, Lehuédé P, Vallotto M, Nardone M, et al. Soda-lime-silica glass containers: chemical durability and weathering products. In: *9th conference of the European-Society-of-Glass-Science-and-Technology/annual meeting of the International-Commission-on-Glass, Trencin, Slovakia.* 2008. p. 305.
17. Rio S, Andraud C, Deniard P, Dacquin C, Delaval R, Donze S, et al. Study of the influence of crystalline phases on optical characteristics of a glass-ceramic in the visible range via simulations by the four-flux method. *J Non-Cryst Solids.* 2021;551:120446.
18. Freude D, Haase J. Excitation of quadrupolar nuclei in solids. In: *NMR Basic Principles and Progress*, Vol. 29. Springer-Verlag, Berlin Heidelberg 1993;15–22.
19. Frugier P, Gin S, Minet Y, Chave T, Bonin B, Godon N, et al. Son68 nuclear glass dissolution kinetics: current state of knowledge and basis of the new Graal model. *J Nucl Mater.* 2008;380:8–21.
20. Fournier M, Ull A, Nicoleau E, Inagaki Y, Odorico M, Frugier P, et al. Glass dissolution rate measurement and calculation revisited. *J Nucl Mater.* 2016;476:140–54.
21. Bunker BC. Molecular mechanisms for corrosion of silica and silicate-glasses. *J Non-Cryst Solids.* 1994;179:300–308.
22. Sinton CW, LaCourse WC. Experimental survey of the chemical durability of commercial soda-lime-silicate glasses. *Mater Res Bull.* 2001;36:2471–79.
23. Aréna H, Rébiscoul D, Garcès E, Godon N. Comparative effect of alkaline elements and calcium on alteration of international simple glass. *NPJ Mater Degrad.* 2019;3:10.
24. Collin M, Fournier M, Charpentier T, Moskura M, Gin S. Impact of alkali on the passivation of silicate glass. *NPJ Mater Degrad.* 2018;2:16.
25. Angeli F, Gaillard M, Jollivet P, Charpentier T. Influence of glass composition and alteration solution on leached silicate glass structure: a solid-state NMR investigation. *Geochim Cosmochim Acta.* 2006;70:2577–90.
26. Perera G, Doremus RH. Dissolution rates of commercial soda-lime and pyrex borosilicate glasses—influence of solution pH. *J Am Ceram Soc.* 1991;74:1554–58.
27. Angeli F, Jollivet P, Charpentier T, Fournier M, Gin S. Structure and chemical durability of lead crystal glass. *Environ Sci Technol.* 2016;50:11549–58.
28. Brunauer S, Emmett PH, Teller E. Adsorption of gases in multimolecular layers. *J Am Chem Soc.* 1938;60:309–19.
29. Soleilhavoup A, Delaye JM, Angeli F, Caurant D, Charpentier T. Contribution of first-principles calculations to multinuclear NMR analysis of borosilicate glasses. *Magn Reson Chem.* 2010;48:S159–70.
30. Fournier M, Odorico M, Nicoleau E, Ull A, Frugier P, Gin S. Reactive surface of glass particles under aqueous corrosion. In: *15th water-rock interaction international symposium (WRI), Evora, Portugal.* 2016. p. 257–60.
31. Ngo D, Liu HS, Sheth N, Lopez-Hallman R, Podraza NJ, Collin M, et al. Spectroscopic ellipsometry study of thickness and porosity of the alteration layer formed on international simple glass surface in aqueous corrosion conditions. *NPJ Mater Degrad.* 2018;2:20.
32. Aspnes DE, Theeten JB, Hottier F. Effective medium description of surface-roughness on amorphous Si from 1.5 to 5.8 Ev. *Bull Am Phys Soc.* 1979;24:278–278.

## SUPPORTING INFORMATION

Additional supporting information can be found online in the Supporting Information section at the end of this article.

**How to cite this article:** Brunswic L, Angeli F, Gautron L, Charpentier T, Gin S, Asplanato P, et al. Structure and durability of opal crystallized glass plates. *Int J Appl Glass Sci.* 2024;e16698.  
<https://doi.org/10.1111/ijag.16698>